

Article

A First-Principles Exploration of Na_xS_y Binary Phases at 1 atm and Under Pressure

Nisha Geng¹, Tiange Bi¹ , Niloofar Zarifi¹, Yan Yan^{1,2} and Eva Zurek^{1,*} ¹ Department of Chemistry, University at Buffalo, Buffalo, NY 14260, USA² School of Sciences, Changchun University, Changchun 130022, China

* Correspondence: ezurek@buffalo.edu

Received: 1 August 2019; Accepted: 20 August 2019; Published: 24 August 2019



Abstract: Interest in Na-S compounds stems from their use in battery materials at 1 atm, as well as the potential for superconductivity under pressure. Evolutionary structure searches coupled with Density Functional Theory calculations were employed to predict stable and low-lying metastable phases of sodium poor and sodium rich sulfides at 1 atm and within 100–200 GPa. At ambient pressures, four new stable or metastable phases with unbranched sulfur motifs were predicted: Na_2S_3 with $C2/c$ and $Imm2$ symmetry, $C2\text{-Na}_2\text{S}_5$ and $C2\text{-Na}_2\text{S}_8$. Van der Waals interactions were shown to affect the energy ordering of various polymorphs. At high pressure, several novel phases that contained a wide variety of zero-, one-, and two-dimensional sulfur motifs were predicted, and their electronic structures and bonding were analyzed. At 200 GPa, $P4/mmm\text{-Na}_2\text{S}_8$ was predicted to become superconducting below 15.5 K, which is close to results previously obtained for the β -Po phase of elemental sulfur. The structures of the most stable M_3S and M_4S , $\text{M} = \text{Na}$, phases differed from those previously reported for compounds with $\text{M} = \text{H}, \text{Li}, \text{K}$.

Keywords: high-pressure; crystal structure prediction; electronic structure; battery materials; superconductivity

1. Introduction

At atmospheric pressures, the size of the metal atom is thought to be important in determining the alkali metal polysulfide stoichiometries that are stable. In the case of the lightest alkali, lithium, only Li_2S and Li_2S_2 have been made [1], whereas for the heavier metal atoms ($\text{M} = \text{K}, \text{Rb}, \text{Cs}$) the known phases include M_2S_n with $n = 1\text{--}6$ [2–5]. The solid state Na-S system is particularly fascinating, with manuscripts reporting the failed synthesis of previously published stoichiometries, or the synthesis of new polymorphs. Na_2S , Na_2S_2 , Na_2S_4 and Na_2S_5 are stable or metastable at atmospheric conditions [2,6–8]. Two polymorphs of Na_2S_2 are known: the α form with three formula units per cell that is stable below 170 °C, and the higher temperature β form with two formula units per cell [9]. Several studies have failed to synthesize or isolate Na_2S_3 , with the reaction products yielding a mixture of Na_2S_2 and Na_2S_4 instead [6]. A novel synthesis route in liquid ammonia yielded Na_2S_3 , but the product decomposed around 100 °C [10]. The crystal structure of $\alpha\text{-Na}_2\text{S}_5$ has been solved [11], and several metastable polymorphs with this stoichiometry have been detected via Raman spectroscopy [2] and X-ray diffraction [8], but their structures were not determined. This amazing structural versatility is in part due to the ability of sulfur to form anionic polysulfide chains, S_n^{2-} , with various lengths. Only unbranched chains are found in the sodium polysulfides, but they may have different arrangements or conformations.

Research on the Na-S system has been motivated by Kummer and Weber's development of the battery containing these two elements at the Ford Motor Company in 1966 [12–14]. The advantages of the Na-S battery include the fact that it is made from inexpensive materials, has a long cycle lifetime,

and it can deliver high-energy densities [15–18]. Density functional theory (DFT) calculations [19–21] and experiments [20] have been carried out to study the ambient pressure phases with Na_2S_n , $n > 1$. Momida and co-workers only considered the known phases. They found that the inclusion of dispersion, as implemented in Grimme's PBE-D2 functional, did not substantially influence their structural parameters nor their energies, in contrast to the results for elemental sulfur [19]. DFT calculations have concluded that, based upon the energy alone, β - Na_2S_2 is somewhat more stable than α - Na_2S_2 [19,20]. Crystal structure prediction (CSP) techniques coupled with DFT calculations have been employed to search for new ambient pressure phases [20,21]. Mali and co-workers computed the enthalpies of formation of the novel $Cmme$ - Na_2S_3 and $C2$ - Na_2S_6 phases, and found that they lay only slightly above the convex hull, suggesting these crystalline lattices may be metastable. A novel low energy polymorph of Na_2S_5 was predicted, and a higher energy ϵ polymorph was synthesized. Both of these were computed to be more stable than the known α phase. Wang and co-workers predicted a new polymorph, γ - Na_2S_2 , which was somewhat higher in energy than the known α and β forms [21]. Moreover, a $C2/c$ symmetry Na_2S_3 structure, which contained V-shaped S_3^{2-} units, was found to be thermodynamically and dynamically stable.

The pressure induced structural transitions, as well as the electronic and optical properties of the dialkali sulfides have been studied extensively. At ambient conditions, Li_2S , Na_2S , K_2S and Rb_2S assume the antifluorite (anti- CaF_2) structure [22,23], whereas Cs_2S crystallizes in an anticottunite (anti- PbCl_2) structure [24]. Li_2S and Na_2S transform to an isotypic anticottunite phase at 12 GPa [25], and 7 GPa [26]. A further transition to an Ni_2In phase occurs at 30–45 GPa [27] and 16 GPa [26] in these systems, respectively. The sequence of phase transitions for Rb_2S are: anti- $\text{CaF}_2 \rightarrow$ anti- $\text{PbCl}_2 \rightarrow \text{Ni}_2\text{In}$ at 0.7 and 2.6 GPa [28]. Cs_2S assumes a distorted Ni_2In structure by 5 GPa [29]. Many of these phase transitions were either predicted or confirmed via theoretical calculations [30]. Recently, CSP has been used to search for the most stable structures of Li_2S , Na_2S [31], and K_2S at higher pressures [31,32]. Na_2S was predicted to transform into an anti- AlB_2 phase at 162 GPa, and an anti- KHg_2 structure at 232–244 GPa [31].

The discovery of conventional superconductivity in a hydride of sulfur that has been identified as $Im\bar{3}m$ - H_3S has invigorated the quest for high-temperature superconductors with unique stoichiometries [33]. The superconducting critical temperature, T_c , measured for this material was a record breaking 203 K at 150 GPa [34]. Because the valence shells of the alkali metal hydrides are isoelectronic with hydrogen, Kokail and co-workers hypothesized that the alkali sulfides could also be good superconductors [35]. CSP was employed to search for stable structures in the metal rich Li-S [35], and K-S [36] phase diagrams under pressure, however most of the phases found had no or low T_c . The only exception was a $Fm\bar{3}m$ - Li_3S structure whose T_c reached a maximum of 80 K at 500 GPa, a pressure at which it was metastable [35].

Herein, we carry out a comprehensive theoretical investigation that employs an evolutionary structure search to predict the most stable, and low-lying metastable phases in the metal rich and metal poor regions of the Na-S phase diagram at 1 atm, as well as 100–200 GPa. In addition to identifying many of the known or previously predicted ambient pressure phases, novel polymorphs with the Na_2S_3 , Na_2S_5 , and Na_2S_8 stoichiometries, which could potentially be synthesized, are found, and their properties are reported. Dynamically stable Na_3S and Na_4S phases, whose structures are related to the antifluorite Na_2S phase, lie ~ 70 meV/atom above the 0 GPa convex hull. (Meta)stable structures in the sulfur rich region of the phase diagram at 100 GPa contain a wide range of sulfur motifs including: zero-dimensional dimers or trimers, one-dimensional zigzag or branched tertiary chains, as well as fused square or cyclohexane motifs. By 200 GPa, most of the predicted phases are comprised of two-dimensional square nets or cubic-like lattices. The most stable Na_3S and Na_4S phases at 200 GPa did not bear any resemblance to H_3S [37], or the sulfides of lithium [35] and potassium [36] whose superconducting properties have previously been investigated. We hope the structural diversity of the phases predicted herein inspires the directed synthesis of new sulfides of sodium.

2. Computational Details

Evolutionary structure searches were carried out to find stable and low-lying metastable crystals in the Na-S phase diagram: in the sulfur rich region the Na_2S_n stoichiometry with $n = 2-6, 8$, and in the metal rich region the Na_nS stoichiometry with $n = 2-4$ were considered. The calculations were carried out using the open-source evolutionary algorithm (EA) XTALOPT [38,39] version 10 [40], wherein duplicate structures were removed from the breeding pool via the XTALCOMP algorithm [41], and random symmetric structures were created in the first generation using RANDSPG [42]. EA searches were performed on structures containing 1–4 formula units in the primitive cell at 0, 100, 150 and 200 GPa. Minimum interatomic distance constraints were chosen to generate the starting structures in each generation. The minimum distances between Na-Na, Na-S and S-S atoms were set to 1.86, 1.45, and 1.04 Å, respectively. To improve the efficiency of the CSP searches, and increase the size of the unit cell that could be considered, the evolutionary search was seeded with experimentally determined and theoretically predicted structures from the literature, when available. The most stable structures found in the high pressure EA searches were optimized between 100 and 200 GPa, and their relative enthalpies and equations of states (EOS) are provided in the Supplementary Materials.

Geometry optimizations and electronic structure calculations including the densities of states (DOS), band structures, electron localization functions (ELFs) and Bader charges were carried out using DFT as implemented in the Vienna *Ab-Initio* Simulation Package (VASP) [43,44]. The bonding of select phases was further analyzed by calculating the crystal orbital Hamilton populations (COHP) and the negative of the COHP integrated to the Fermi level (-iCOHP) using the LOBSTER package [45]. At all pressures, the gradient-corrected exchange and correlation functional of Perdew–Burke–Ernzerhof (PBE) [46] was employed. It has been shown that it is important to include van der Waals (vdW) interactions to obtain reasonable estimates for the volume of α -S at 1 atm [19]. Therefore, the most stable structures from the 0 GPa PBE EA searches were reoptimized with the optB88-vdW functional [47,48]. In the EA searches, we employed plane-wave basis set cutoff of 325–400 eV, and the k -point meshes were produced by the Γ -centered Monkhorst–Pack scheme with the number of divisions along each reciprocal lattice vector chosen so that the product of this number with the real lattice constant was 30 Å. This value was increased to 50 Å for precise optimizations. The atomic potentials were described using the projector augmented wave (PAW) method [49]. The S $3s^23p^4$ electrons were treated explicitly in all of the calculations. At 0 GPa the Na $3s^1$ valence electron configuration was used, and at higher pressures an Na $2s^22p^63s^1$ valence configuration was employed. For precise optimizations, the plane-wave basis set cutoffs were increased to 700 eV at 0 GPa, and 1000 eV at high pressures.

To verify the dynamic stability phonon band structures were calculated via the supercell approach [50,51], wherein the dynamical matrices were calculated using the PHONOPY code [52]. The electron–phonon coupling (EPC) calculations were performed using the Quantum Espresso (QE) program [53]. The Na ($2s^22p^63s^1$) and S ($3s^23p^4$) pseudopotentials, obtained from the PSLibrary [54], were generated by the method of Trouiller–Martins [55] with the PBE functional, and an energy cutoff of 90 Ry was chosen. The Brillouin zone sampling scheme of Methfessel–Paxton [56] and $24 \times 24 \times 6$ k -point grid and a $8 \times 8 \times 2$ q -point grid were used for $P4/mmm$ Na_2S_8 at 200 GPa. The EPC parameter, λ , was calculated using a set of Gaussian broadenings with an increment of 0.02 Ry from 0.0 to 0.600 Ry. The broadening for which λ was converged to within 0.05 Ry was 0.10 Ry. T_c was estimated using the Allen–Dynes modified McMillan equation [57] with a renormalized Coulomb potential, μ^* , of 0.1.

3. Results and Discussion

3.1. Stable and Metastable Na-S Phases at Atmospheric Conditions

The enthalpies of formation, ΔH_F , of the most stable Na-S phases found in our EA searches are plotted in Figure 1 as a function of pressure. The phases whose ΔH_F lie on the convex hull are thermodynamically stable, while those whose ΔH_F are not too far from the hull may be metastable

stable provided their phonon modes are all real. At atmospheric pressures, calculations carried out with both the PBE and optB88-vdW functionals showed that the Na_2S , Na_2S_2 , Na_2S_4 and Na_2S_5 stoichiometries lay on the hull. The ΔH_F of Na_2S_3 , Na_2S_6 and Na_2S_8 were slightly above the hull, whereas those of Na_3S and Na_4S were further away from it. The inclusion of vdW interactions lowered the total ΔH_F by no more than 80 meV/atom, but the stoichiometries that lay on the hull were the same as those found within PBE. The inclusion of the zero point energy, ZPE, increased the ΔH_F by no more than 9 meV/atom, but it also did not affect the identities of the thermodynamically stable phases. The structural parameters and ΔH_F of the stable and important metastable phases are provided in the Supplementary Materials. All of the structures identified in the EA search that were within 15 meV/atom of the lowest enthalpy geometry for a particular stoichiometry were examined, and none of them contained sulfur anions with branched chains.

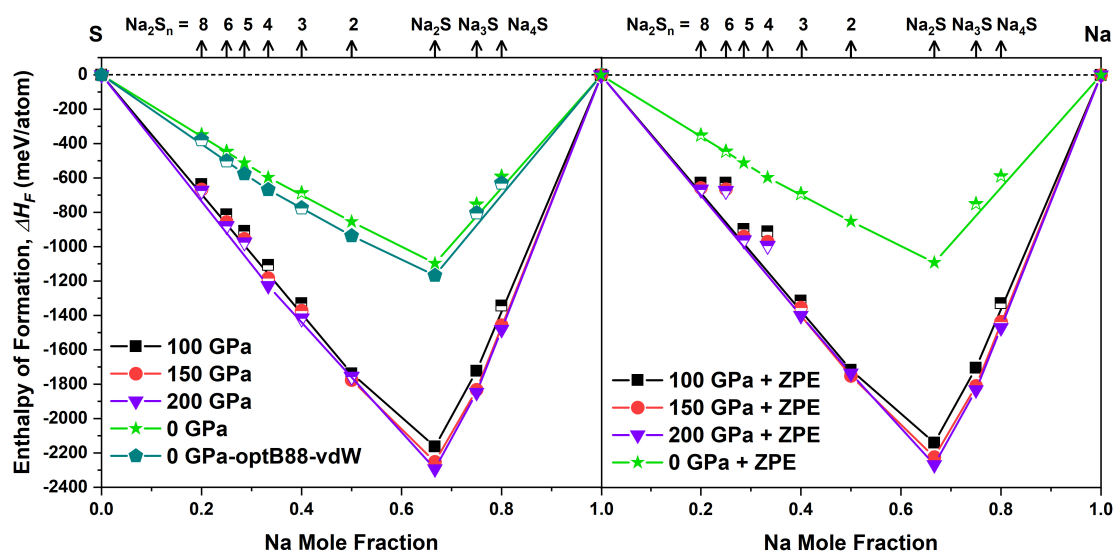


Figure 1. (left) Enthalpy of formation, ΔH_F , of the Na_xS_y compounds with respect to solid Na and S as computed with the optB88-vdW functional at 0 GPa and the PBE functional between 0–200 GPa. (right) PBE results including the zero point energy (ZPE). Closed symbols lie on the convex hull (denoted by solid lines), open symbols lie above it. ΔH_F was calculated using the enthalpies of the experimentally known structures: body-centered cubic (bcc, 0 GPa), face-centered cubic (fcc, 100 GPa) [58], *cI16* (150 GPa) [59,60], and *hp4* (200 GPa) [61] for Na, and α -S (0 GPa) [62]. Because the crystal structure of S above 83 GPa is still disputed [63,64], the β -Po phase [65] was employed between 100 and 200 GPa, as in recent studies [35].

Momida [19] and Wang et al. [21] studied the effect of vdW interactions on the unit cell volumes and formation enthalpies of the sodium polysulfides. The effects of dispersion were approximated by using Grimme's semi-empirical DFT-D2 method [66] in conjunction with the PBE functional. Both studies found that vdW interactions resulted in slightly smaller volumes for the Na-S compounds, and more negative formation enthalpies. However, the inclusion of dispersion was crucial so that reasonable estimates of the unit cell volume of elemental α -S, which is composed of molecular S_8 rings, could be calculated [19]. Herein, the optB88-vdW method [47,48], which employs a non-local correlation functional that approximately accounts for dispersion interactions, was used. It has been demonstrated that this functional is among those that provides the best agreement with experiment for the volumes and lattice constants of layered electroactive materials for Li-ion batteries [67], as well as a broad range of metallic, covalent and ionic solids [48]. Other choices that might provide even more accurate lattice parameters at ambient pressures include combining PBE [46], and PBEsol [68] or its improvements [69] with rVV10 [70,71], or SCAN+rVV10 [72]. A comparison of the calculated volumes per atom obtained via PBE and optB88-vdW are provided in the Supplementary Materials. For elemental sulfur, PBE yields a cell volume of $37.21 \text{ \AA}^3/\text{atom}$, which is 36.4% larger

than the experimental volume of $25.76 \text{ \AA}^3/\text{atom}$ [73]. The optB88-vdW functional yields a volume of $24.90 \text{ \AA}^3/\text{atom}$ (c.f. $26.88 \text{ \AA}^3/\text{atom}$ with PBE-D2 [19]), which is only 3.4% lower than experiment. In Na-S systems that contained at least 50 mole % sodium, the difference between the PBE and optB88-vdW volumes was $<4\%$, otherwise the difference ranged from 5–16%, depending on the stoichiometry and polymorph. For Na_2S , $\alpha\text{-Na}_2\text{S}_2$, $\beta\text{-Na}_2\text{S}_2$, Na_2S_4 , and Na_2S_5 optB88-vdW yielded volumes of 22.77, 21.51, 21.90, 21.85, and $22.38 \text{ \AA}^3/\text{atom}$, respectively, which differs by $<4\%$ from Momida's PBE-D2 results [19]. The 0 K optB88-vdW ΔH_F values for the most stable Na_2S , Na_2S_2 , Na_2S_4 , and Na_2S_5 polymorphs were calculated to be -1.17 , -0.94 , -0.67 , and -0.58 eV/atom , which is in good agreement with the experimental ΔH_F^0 values at 298.15 K of -1.26 , -1.03 , -0.71 , and -0.61 eV/atom , respectively [74].

The anti- CaF_2 Na_2S structure with $Fm\bar{3}m$ symmetry was the lowest point on the 0 GPa convex hull [19–21], and the Na_2S_2 stoichiometry had the second most negative ΔH_F . Our EA searches were seeded only with the known α and $\beta\text{-Na}_2\text{S}_2$ polymorphs, but they also readily identified a higher energy $\gamma\text{-Na}_2\text{S}_2$ phase that has recently been predicted [21]. All of these three polymorphs are comprised of Na^+ cations and S_2^- anions. In agreement with previous DFT calculations [19–21], the β polymorph was computed to have the lowest ΔH_F , followed by the α , and the γ configurations. The PBE/optB88-vdW differences in energy between the α and β structures were comparable to the difference between the β and γ structures, $4/8 \text{ meV/atom}$ and $5/9 \text{ meV/atom}$, respectively.

In addition to Na_2S and Na_2S_2 , the Na_2S_4 and Na_2S_5 stoichiometries also lay on the PBE and optB88-vdW convex hulls. The EA search was seeded with the known $\bar{I}42d\text{-Na}_2\text{S}_4$ structure [75], which contains an unbranched S_4^{2-} chain whose S-S bond angle and dihedral angle were computed to be 111.3° and 96.7° , within PBE, respectively. No other polymorphs with comparable energies were found.

The EA search was also seeded with the $\alpha\text{-Na}_2\text{S}_5$ [11] and $\epsilon\text{-Na}_2\text{S}_5$ [20] polymorphs illustrated in Figure 2a,b. In the α form, the unbranched S_5^{2-} anion adopts a bent (*cis*) configuration, whereas, in the ϵ form, it is stretched (*trans*), as in K_2S_5 [76], Rb_2S_5 [77] and Cs_2S_5 [78]. PBE and PBE-D2 calculations have shown that neither the α nor the ϵ phases lay on the convex hull [19,20], but CSP has found another currently unsynthesized phase with stretched S_5^{2-} anions that was thermodynamically stable [20]. The coordinates of this phase were not provided in Ref. [20], however it appears to be different from the lowest enthalpy C2 symmetry Na_2S_5 phase from our EA searches shown in Figure 2c. In the structure of Mali and co-workers [20], neighboring S_5^{2-} chains point in opposite directions (similar to what is observed in the ϵ phase along the *b*-lattice vector), whereas in C2- Na_2S_5 they face the same direction. C2- Na_2S_5 lay on the PBE convex hull, and its enthalpy was 4 and 5 meV/atom lower than the ϵ and α polymorphs, respectively. The order of stability was not affected by the ZPE contributions. On the other hand, within optB88-vdW, the ϵ phase, which lay on the convex hull, had the lowest enthalpy with the α and C2 phases being 3 and 25 meV/atom higher, respectively. These results suggest that other energetically competitive polymorphs, based upon unbranched S_5^{2-} units with either *cis* or *trans* geometries, could potentially be constructed, and that the computed energy ordering depends upon the method used to treat dispersion. PBE calculations showed that all three Na_2S_5 polymorphs had indirect band gaps with values of 1.73, 1.47, and 1.30 eV for the ϵ , α , and C2 phases, respectively (see the Supplementary Materials). Better estimates could be obtained using hybrid density functionals or GW, however the PBE results suggest that the conformation of the S_5^{2-} anion and the geometry of the cell both have an effect on the band gap.

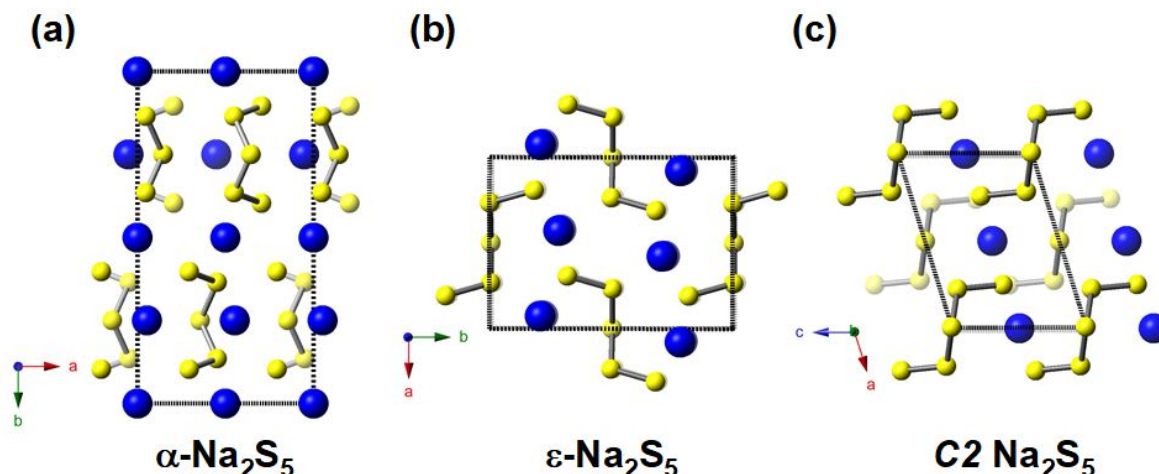


Figure 2. Unit cells of the previously known (a) α - Na_2S_5 [11] and (b) ϵ - Na_2S_5 [20] polymorphs, as well as the newly predicted (c) $\text{C2-Na}_2\text{S}_5$ structure. Sodium atoms are colored blue, and sulfur atoms are yellow.

Besides the previously mentioned thermodynamically stable stoichiometries, several sulfur-rich containing phases, Na_2S_n ($n = 3, 6, 8$), were found to be low-energy metastable species, as confirmed by phonon calculations. For the Na_2S_3 stoichiometry, the Cmme , $\text{C2}/c$ -I, $\text{C2}/c$ -II, and Imm2 polymorphs illustrated in Figure 3 lay 7/22, 3/1, 13/9, and 17/40 meV/atom above the convex hull within PBE/optB88-vdW calculations. CSP previously predicted the Cmme [20] and $\text{C2}/c$ -I [21] structures, used as seeds in our EA searches, whereas the $\text{C2}/c$ -II and Imm2 phases discovered here have not been reported before. All four of these polymorphs contained V-shaped S_3^{2-} anions with S-S bond lengths of 2.087–2.107 Å and bond angles of 106.00–111.21°. The main difference between them was the relative arrangement of the S_3^{2-} motifs. In Imm2 all of the V-shaped anions pointed in the same direction, whereas in $\text{C2}/c$ -II those in a single layer pointed in the same direction, but those in the adjacent layer were rotated by 180°. In Cmme and $\text{C2}/c$ -I adjacent rows of anions in the same layer pointed in opposite directions. In Cmme the apex of the Vs in one layer were located directly behind those in an adjacent layer, but rotated by 180°. In $\text{C2}/c$ -I, the Vs in adjacent layers also faced opposite directions. All four polymorphs had indirect band gaps, with the PBE value for $\text{C2}/c$ -I, 1.06 eV, being about 0.5 eV smaller than for the other three. The closeness of the ΔH_F of these four polymorphs to the convex hull, and their dynamic stability suggests that they may be synthesizable. Experimentalists have not yet been able to synthesize a persistent Na_2S_3 compound, yielding a mixture of Na_2S_4 and Na_2S_5 either directly [6,20,79] or after disproportionation near 100 °C [10], suggesting that the kinetic barriers towards decomposition may be low.

Seed structures were not employed in EA searches carried out on the Na_2S_6 stoichiometry, and the two nearly isoenthalpic C2 and $\text{P}\bar{1}$ symmetry structures illustrated in Figure 4a,b were found. Whereas the former was comprised of unbranched S_6^{2-} units, the latter contained V-shaped trimers. These two dynamically stable phases lay only 2/3 and 5/16 meV/atom above the PBE/optB88-vdW convex hulls, respectively. The inclusion of the ZPE decreased the PBE difference in energy to 1 meV/atom. Mali and co-workers found the same two structures in their CSP searches [20]. The calculated phonon spectrum of $\text{P}\bar{1}$ - Na_2S_6 contained two bands above 500 cm^{-1} (565 and 543 cm^{-1} at Γ), which is higher than in any of the other 0 GPa phase considered herein. The S-S bond distances in $\text{P}\bar{1}$ - Na_2S_6 were shorter than in any of the predicted Na_2S_3 phases, 1.972 and 2.048 Å, giving rise to the increased frequency. The decreased distance is likely a result of the smaller formal charge on the trimer, S_3^- in $\text{P}\bar{1}$ - Na_2S_6 vs. S_3^{2-} in the Na_2S_3 polymorphs in Figure 3. Molecular calculations using the ADF program package [80,81] with a triple-zeta basis set with polarization functions (TZP), and the PBE functional yielded S-S bond lengths of 2.037 and 2.166 Å in the monoanion and dianion, respectively, which is in

reasonable agreement with the periodic calculations. Both phases were computed to have indirect PBE band gaps, 1.75 eV in the $C2$ and 0.72 eV in the $P\bar{1}$ phases, respectively.

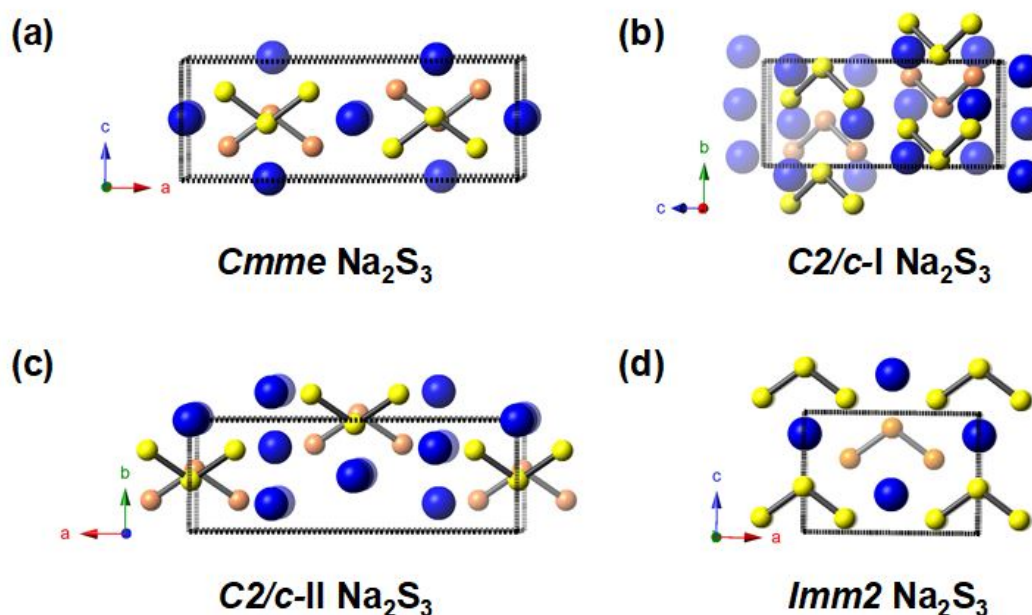


Figure 3. Unit cells of the previously predicted (a) $Cmme$ - Na_2S_3 [20], and (b) $C2/c$ -I Na_2S_3 [21] phases, as well as the newly found (c) $C2/c$ -II Na_2S_3 , and (d) $Imm2$ - Na_2S_3 geometries. Sodium atoms are colored blue, whereas sulfur atoms in adjacent layers are yellow and orange.

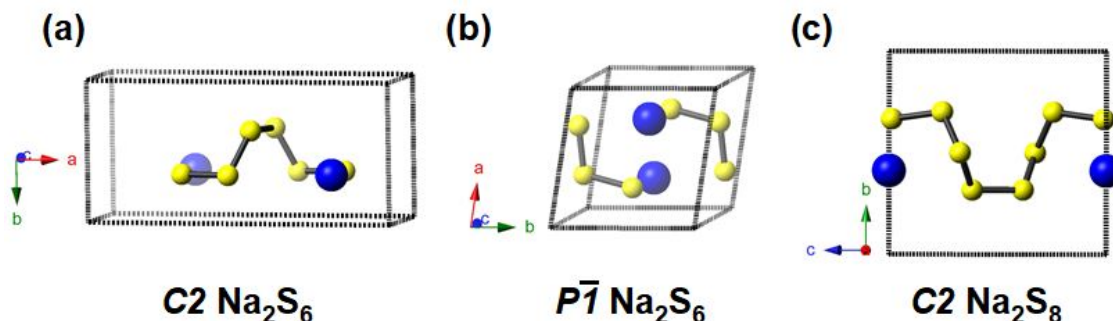


Figure 4. Unit cells of the previously predicted (a) $C2$ - Na_2S_6 [20], and (b) $P\bar{1}$ - Na_2S_6 polymorphs. (c) Unit cell of the newly predicted $C2$ - Na_2S_8 phase. Sodium atoms are colored blue, and sulfur atoms are yellow.

Finally, EA searches were carried out on the Na_2S_8 stoichiometry, which has not been considered in other studies before. The dynamically stable $C2$ symmetry structure shown in Figure 4c was found to have the lowest energy and it lay 10/30 meV/atom above the PBE/optB88-vdW convex hulls. This phase is comprised of an unbranched S_8^{2-} stretched, helical-like chain. Its PBE band gap was indirect and measured 1.56 eV.

Two sodium rich metastable phases, whose structures can be derived from the known 1 atm $Fm\bar{3}m$ - Na_2S configuration, which has one formula unit per primitive cell and is shown in Figure 5a, were found. The $P\bar{3}m1$ - Na_3S and $Pmn2_1$ - Na_4S phases illustrated in Figure 5b,c lay 69/71 and 67/70 meV/atom above the PBE/optB88-vdW convex hull, respectively. In the antifluorite Na_2S structure the S^{2-} anions are arranged on a face centered cubic (fcc) lattice, and all of the tetrahedral sites are filled with Na^+ cations, with the Na-Na nearest neighbor distances measuring 3.267 Å. The $P\bar{3}m1$ - Na_3S phase can be derived from a three-formula unit supercell of the antifluorite structure

where one sulfur atom has been removed from the fcc lattice. This results in a distortion from perfect cubic symmetry, with Na-Na-Na angles measuring 89.3 and 89.9°, and Na-Na nearest neighbor distances measuring 3.288 and 3.242 Å. Another dynamically stable $R\bar{3}m$ symmetry phase that was 0.7/1.5 meV/atom less stable within PBE/optB88-vdW was also found in the structure searches. Its coordinates and computed properties are provided in the Supplementary Materials. The $Pmn2_1$ -Na₄S structure contained four formula units. It can be obtained by inserting layers of sodium atoms into a supercell of the antifluorite structure, which results in a minimal structural distortion in the anti-CaF₂ layers, with Na-Na distances along the *a* and *c* lattice vectors measuring 3.344 and 3.267 Å, respectively.

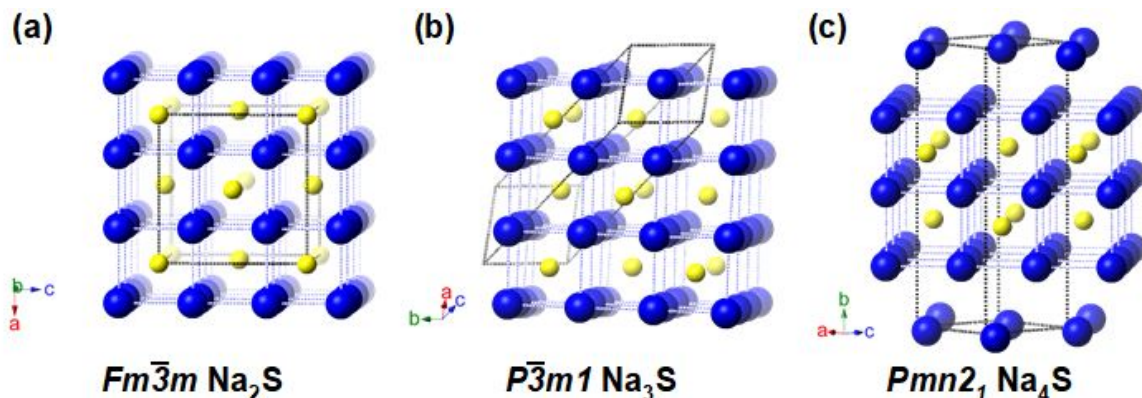


Figure 5. Crystal structures of (a) $Fm\bar{3}m$ -Na₂S, (b) $P\bar{3}m1$ -Na₃S and (c) $Pmn2_1$ -Na₄S phases at 0 GPa. Sodium atoms are colored blue, and sulfur atoms are yellow.

The PBE band gap in $Fm\bar{3}m$ -Na₂S was computed to be 2.47 eV, as expected for an ionic phase. As shown in the Supplementary Materials, the sodium rich $P\bar{3}m1$ -Na₃S and $Pmn2_1$ -Na₄S compounds are metals. Plots of the ELF, given in Figure 6, illustrate that regions where the bonding is metallic, indicated by an ELF value of ~ 0.5 , are localized along the two-dimensional layers of sodium atoms. The DOS of both structures between -2.5 eV to the Fermi level has step-like features, as would be expected for a two-dimensional electron gas [82]. The ELF plots also show spherical regions with high ELF values that encompass the sulfur atoms, suggestive of an S²⁻ oxidation state, and regions with a high ELF value between adjacent Na layers within $Pmn2_1$ -Na₄S. The latter are labeled “Es” in Figure 6d, since they resemble interstitial electrons that are paired in anion-like species, which have been computed for a number of high-pressure electrides exhibiting ionic bonding [83,84].

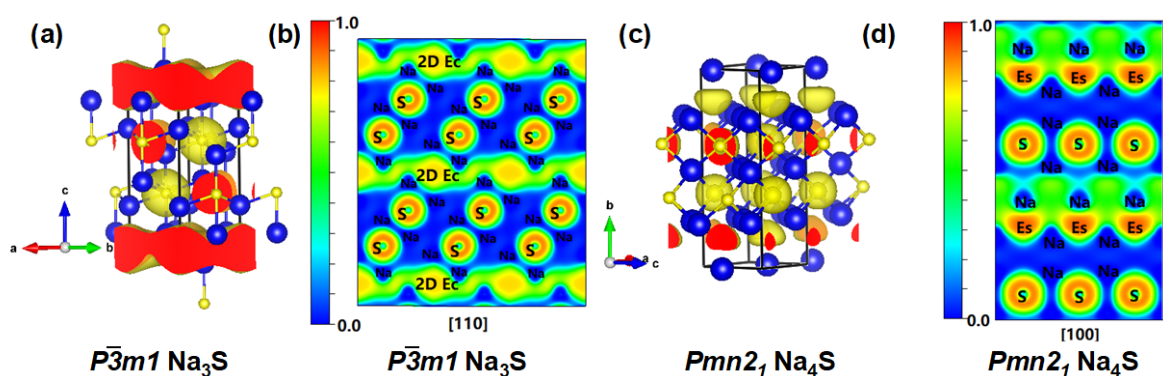


Figure 6. The electron localization function (ELF) plots of sodium rich phases at 0 GPa. $P\bar{3}m1$ -Na₃S: (a) ELF isosurface plot using an isovalue of 0.5, and (b) slice of the ELF in the [100] plane. $Pmn2_1$ -Na₄S: (c) ELF isosurface plot with an isovalue of 0.8, and (d) slice of the ELF in the [110] plane. In the two-dimensional plots, the positions of the S and Na atoms are denoted, as is the plane of the two-dimensional electron cloud (Ec) and the positions of the interstitial electron pairs (Es).

3.2. Na-S System at High Pressure

Because dispersion interactions are unlikely to be important under pressure [85], calculations at 100, 150 and 200 GPa were carried out with the PBE functional. Figure 1 illustrates that only Na₃S and Na₂S were thermodynamically stable at all of these pressures. Na₂S₂ lay on the 100 and 150 GPa convex hulls, whereas Na₄S and Na₂S₄ lay on the 200 GPa convex hull. The inclusion of the ZPE corrections did not affect the identity of the thermodynamically stable stoichiometries at 100 and 150 GPa, but it added Na₂S₂ and Na₂S₃ to the 200 GPa hull, and pushed Na₂S₄ away from it. Because phonon calculations (see the Supplementary Materials) confirmed that all of these phases were dynamically stable, and high-pressure experiments can lead to the formation of metastable species [86]; the structures of all of these phases are discussed below.

The Na₂S stoichiometry was the lowest point on the convex hull among all other binary phases between 100–200 GPa. The species seeded into the EA, including the experimentally known Ni₂In structure (*P6₃/mmc*) [26] and a previously predicted anti-AlB₂ structure (*P6/mmm*) [31] were found to be the most stable at 100–150 GPa and 200 GPa, respectively. DFT calculations have predicted that Na₂S is an insulator up to 300 GPa, with PBE band gaps of ~3.50, 3.25, and 1.70 eV at 100, 150 and 200 GPa, respectively [31].

The evolutionary search for Na₂S₂ at 100–200 GPa found a *Pbam* symmetry structure, shown in Figure 7a, which contained two formula units in its primitive cell. It lay on the convex hull at 100 and 150 GPa, and was only 5 meV/atom away from the hull at 200 GPa. Its shortest S-S distances were no longer than 2.040 Å at all of the pressures studied, which is comparable to the measured S-S bond length within α -S at ambient conditions, 2.055 Å [73]. A plot of the ELF, shown in the Supplementary Materials, confirmed the presence of layers of S₂²⁻ dimers, arranged in a herringbone type fashion.

The Na₂S₃ stoichiometry lay above the convex hull at all pressures considered, however the distance from the hull decreased from 65 to 25 meV/atom from 100 to 200 GPa. The C2/*c* phase shown in Figure 7b, which was metastable between 100 and 150 GPa, is comprised of one-dimensional branched tertiary sulfur chains with S-S distances of 2.180 Å along the chain, and 2.030 Å along the branch. By 150 GPa, the *I4/mmm* structure illustrated in Figure 8a, was enthalpically preferred. It is comprised of two layers of square sulfur nets, with S-S distances of 2.092 Å at 200 GPa, separated by sodium nets.

Na₂S₄ was thermodynamically stable at 200 GPa, but it lay 55 and 3 meV/atom from the 100 and 150 GPa hulls. The most stable structure between 100–110 GPa, shown in Figure 7c, had C2/*c* symmetry and contained layers of hexagonal puckered corner-sharing chair cyclohexane-like rings with S-S distances of 2.105 and 2.232 Å. The Bader charges on the 4- and 2-coordinated sulfur atoms were $-0.16e$ and $-0.60e$, respectively. Above 110 GPa, the *I4/mmm* structure, shown in Figure 8b, was preferred. Similar to *I4/mmm*-Na₂S₃, it was comprised of two sets of two-dimensional square sulfur layers with S-S distances of 2.092 Å at 200 GPa separated by a single square net of sodium atoms.

The stoichiometries with an even larger ratio of sulfur to sodium lay between 35–85 meV/atom from the non-ZPE corrected convex hull. The structure dubbed C2/*m*-I Na₂S₅ was the most stable at 100 GPa, but by 130 GPa another phase with the same symmetry, C2/*m*-II Na₂S₅, became preferred (see Figure 7d,e). At 100 GPa, the sulfur sublattice in the former contained zigzag chains with S-S distances of 2.076 Å, as well as one-dimensional corner sharing squares with S-S distances of 2.194 Å running along the *b*-lattice vector. The higher pressure structure was comprised of these same one-dimensional square nets fused at the edges with S-S distances ranging from 2.029 to 2.070 Å at 200 GPa.

At 100 GPa, the lowest enthalpy Na₂S₆ structure adopted C2 symmetry (see Figure 7f), and it lay 60 meV/atom above the convex hull. It was comprised of sulfur atoms as well as dimers and V-shaped trimers, as shown in the ELF plots in the Supplementary Materials, with S-S bond lengths of 2.062 Å, and 1.998–2.180 Å, respectively. The *I4/mmm* phase illustrated in Figure 8c lay 35 and 45 meV/atom above the hulls at 150 and 200 GPa, respectively. It resembled the high-pressure Na₂S₄

and Na_2S_3 phases, except that its sulfur layers contained both edge-sharing cubes and square nets with S-S distances of 1.916–2.111 Å and 2.111 Å, respectively at 200 GPa.

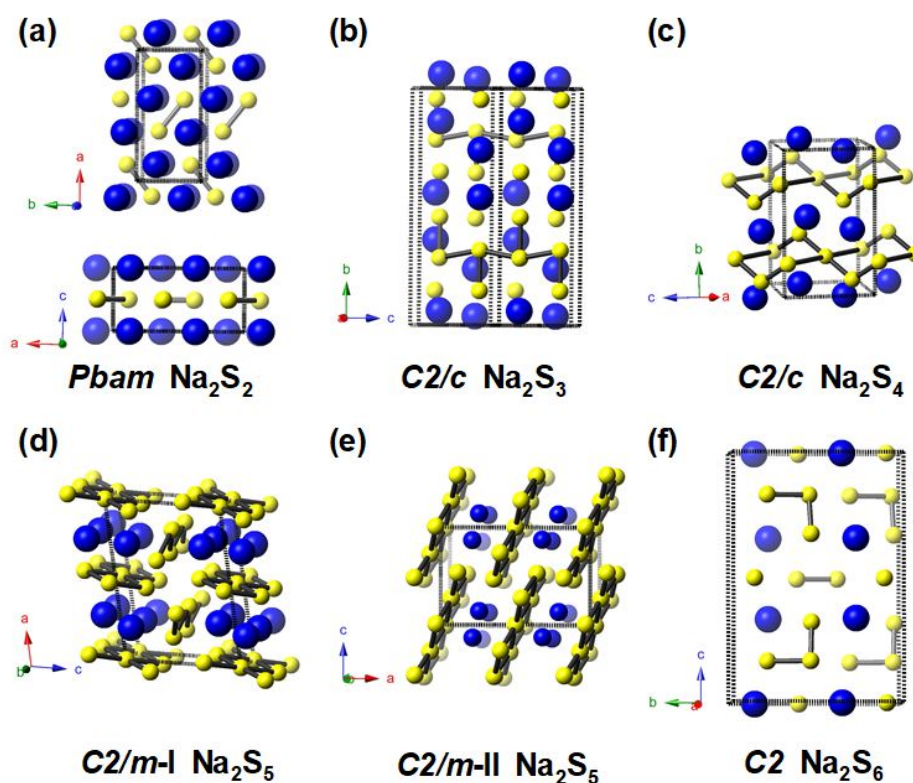


Figure 7. Predicted crystal structures of Na_2S_n ($n = 2-6$) phases under pressure whose sulfur sublattices were comprised of molecular (dimers, trimers) or one-dimensional (chains, corner or edge sharing squares, or corner sharing cyclohexane-like rings) motifs: (a) top and side view of $Pbam\text{-Na}_2\text{S}_2$ at 200 GPa; (b) $C2/c\text{-Na}_2\text{S}_3$ at 100 GPa; (c) $C2/c\text{-Na}_2\text{S}_4$ at 100 GPa; (d) $C2/m\text{-I Na}_2\text{S}_5$ at 100 GPa; (e) $C2/m\text{-II Na}_2\text{S}_5$ at 200 GPa; and (f) $C2\text{-Na}_2\text{S}_6$ at 100 GPa. Sodium atoms are colored blue, and sulfur atoms are yellow.

Evolutionary searches carried out at 100, 150, and 200 GPa for Na_2S_8 discovered the metastable $P4/mmm$ phase shown in Figure 8d. This species was reminiscent of $I4/mmm\text{-Na}_2\text{S}_6$ with layers comprised of fused cubes and square nets with S-S distances of 1.903–2.124 Å and 2.124 Å, respectively, at 200 GPa. ELF plots for $P4/mmm\text{-Na}_2\text{S}_8$ are provided in the Supplementary Materials because they are representative of the ELF plots obtained for phases that contained square and/or cube-like sulfur nets. In all of the structures studied, the ELF plots suggested that the S-S bonds within the two-dimensional sheets were weaker than the bonds between atoms in different sheets. For example, in $P4/mmm\text{-Na}_2\text{S}_8$ the S-S distances along the a - and b -directions were 2.124 Å and the negative of the crystal orbital Hamilton populations integrated to the Fermi level ($-i\text{COHPs}$) were 2.5 eV. For the S-S bonds that were oriented along the c -direction these values became 1.903 Å and 5.5 eV, which is comparable with a bond length of 2.168 Å and $-i\text{COHP}$ of 4.8 eV in the S_2^{2-} dimer in $\alpha\text{-Na}_2\text{S}_2$ at 0 GPa. The pressure induced polymerization and bond weakening observed in the two-dimensional sulfur layers has been seen in other systems before. For example, it has been shown that the Cl_2 molecules present in XeCl at 40 GPa undergo polymerization to form one-dimensional zigzag chains by 60 GPa with the $-i\text{COHPs}$ between nearest neighbor atoms computed to be 3.81 eV and 2.16 eV, respectively [85]. By 100 GPa, however, there is no evidence of Cl-Cl bond formation with computed ELF and $-i\text{COHPs}$ characteristic for monoatomic Cl.

Within the 100–200 GPa pressure range, the most stable Na_3S stoichiometry unearthed contained two formula units in its primitive cell, and it possessed $P6_3/mmc$ symmetry. This structure,

illustrated in Figure 9a, consisted of an ABAB... stacked triangular net where each sulfur atom was [6+6] coordinated with Na-S distances of 2.216 and 2.286 Å at 200 GPa. We also optimized Na₃S stoichiometries that were analogous to the $R\bar{3}m$ and $Im\bar{3}m$ structures proposed for superconducting H₃S [37]; as shown in the Supplementary Materials, their enthalpies were at least 600 meV/atom and 1000 meV/atom higher, respectively, between 100–200 GPa. Moreover, sodium analogs of the previously predicted $Pm\bar{3}m$, $I4/mmm$ and $Fm\bar{3}m$ -Li₃S [35] and $Pm\bar{3}m$, $I4/mmm$ -K₃S [36] phases were relaxed, and they were found to be at least 160 meV/atom less stable than $P6_3/mmc$ -Na₃S between 100 and 200 GPa.

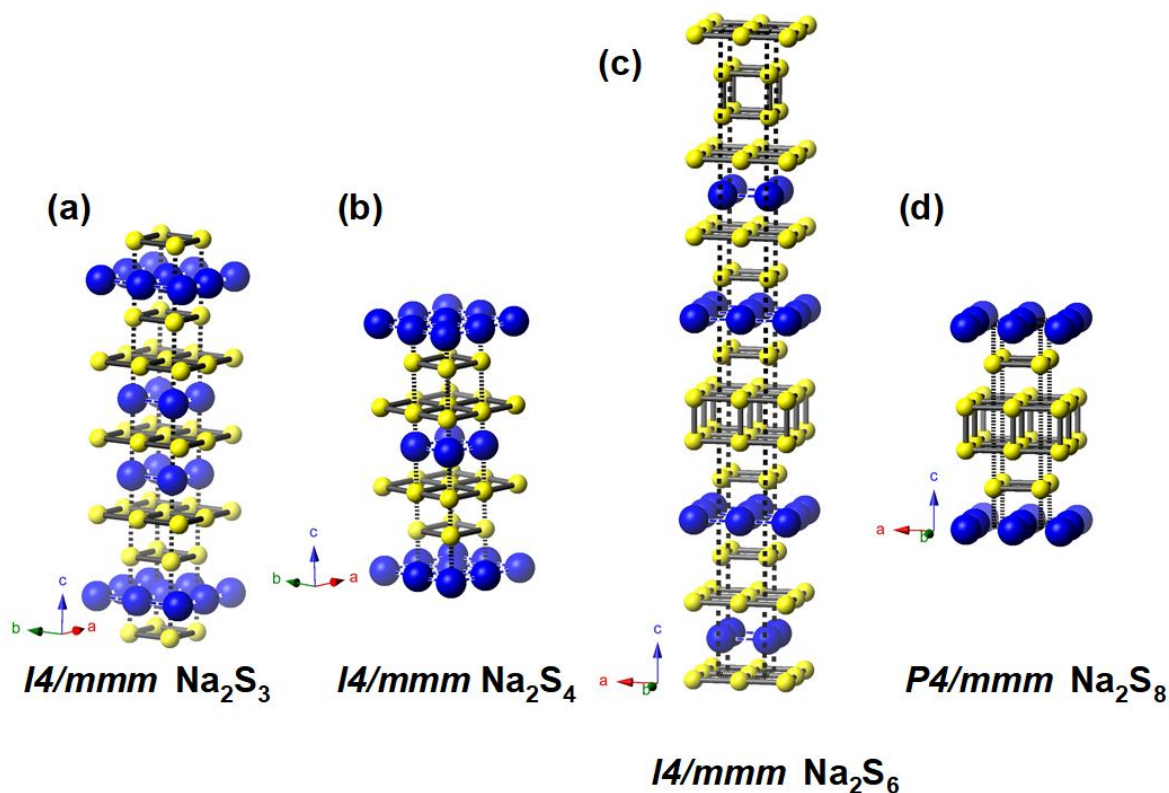


Figure 8. Predicted crystal structures of Na₂S_{*n*} (*n* = 3, 4, 6, 8) phases at 200 GPa whose sulfur sublattices were comprised of two-dimensional square or cube nets, and whose sodium sublattices were comprised of square nets: (a) $I4/mmm$ -Na₂S₃; (b) $I4/mmm$ -Na₂S₄; (c) $I4/mmm$ -Na₂S₆; and (d) $P4/mmm$ -Na₂S₈. Sodium atoms are colored blue, and sulfur atoms are yellow.

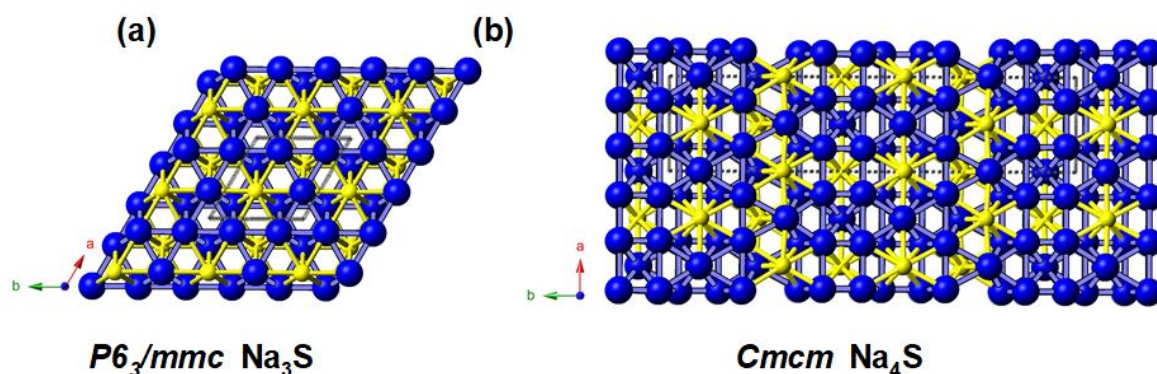


Figure 9. Predicted crystal structures of sodium rich phases at 200 GPa: (a) $P6_3/mmc$ -Na₃S; and (b) $Cmcm$ -Na₄S. Sodium atoms are colored blue, and sulfur atoms are yellow. Blue and yellow lines represent nearest neighbor contacts.

The *Cmcm* symmetry Na_4S phase, shown in Figure 9b, was also found to be the most stable in the whole pressure range of 100–200 GPa. At 200 GPa, it lay on the convex hull, but at 100 and 150 GPa, it was 35 and 10 meV/atom above the hull. It can be viewed as a cut triangular two-dimensional lattice that is joined to another such lattice via a square net. Individual sheets are stacked in an ABAB fashion. Geometry optimizations of the sodium analog of *Cmcm*- K_4S [36] were between 25 and 50 meV/atom less stable than *Cmcm*- Na_4S , whereas the enthalpies of the sodium analogs of *R $\bar{3}m$* - Li_4S [35] and K_4S [36] were at least 200 meV/atom higher than the most stable structure found here.

3.3. Electronic Structure and Superconductivity under Pressure

The PBE band structures and electronic DOS plots of the high-pressure dynamically stable phases, provided in the Supplementary Materials, showed that within their range of stability they were all metallic. Under pressure elemental sodium transforms from the ambient pressure bcc structure to an fcc phase at 65 GPa [58], followed by the semi-metallic *cI16* structure at 103 GPa [87]. Near the minimum of the melting temperature a number of complex crystal structures, with unit cells as large as 512 atoms, have been identified experimentally within a narrow temperature/pressure range [59]. Remarkably, as first predicted by theory [88], sodium undergoes a metal to insulator (MIT) transition by 200 GPa, which results from the overlap of core electrons and the concomitant localization of $p-d$ hybridized valence electrons, which render this phase an electrone [61]. Theoretical calculations have found that the maximum electron–phonon-coupling parameter, λ , for sodium occurs for the *cI16* phase near 140 GPa [89]. Estimates of the T_c within the Allen–Dynes modified McMillan equation and $\mu^* = 0.13$ found a maximum T_c of 1.2 K, leading to the conclusion that superconductivity in sodium prior to the MIT is weak or non-existent. In addition, because DFT calculations showed that most of the metal rich binary lithium and potassium sulfides had no or low T_c [35,36], we thought it unlikely that the *P6 $_3$ /mmc*- Na_3S and *Cmcm*- Na_4S phases found herein would be good superconductors.

In contrast, compressed sulfur is among the elemental phases with the highest T_c , reaching up to 17 K in the rhombohedral β -Po geometry near 160 GPa [90]. The β -Po structure can be viewed as a simple cubic (sc) lattice compressed along the body diagonal, and both can be described using the same unit cell with rhombohedral angles of 90° (sc) and 104° (β -Po) [91]. This made us wonder if the metastable *I4/mmm*- Na_2S_6 or *P4/mmm*- Na_2S_8 phases, which both contained sc-like sulfur layers, could potentially be candidates for conventional superconductivity? Calculations were carried out on the latter since it had a higher sulfur content, and a larger normalized density of states at the Fermi level. Figure 10 shows the computed phonon band structure, Eliashberg spectral function, and the electron–phonon integral for *P4/mmm*- Na_2S_8 . Because of the similar masses of the sodium and sulfur atoms, both atom types contribute to the phonon modes across the frequency spectrum. The EPC was calculated to be $\lambda = 0.79$ and the logarithmic average frequency $\omega_{\log} = 344.8$ K, resulting in a T_c of 15.5 K using a $\mu^* = 0.1$. For comparison, LDA calculations on the β -Po structure at 200 GPa obtained $\lambda = 0.78$ and $T_c = 19.2$ K using the Allen–Dynes approximation with $\mu^* = 0.11$ [91], and $T_c \sim 16$ K via the multiband approach within the superconducting density functional theory (SCDFT) formalism [92]. Thus, the propensity for superconductivity in *P4/mmm*- Na_2S_8 under pressure appears to be similar to that of elemental sulfur.

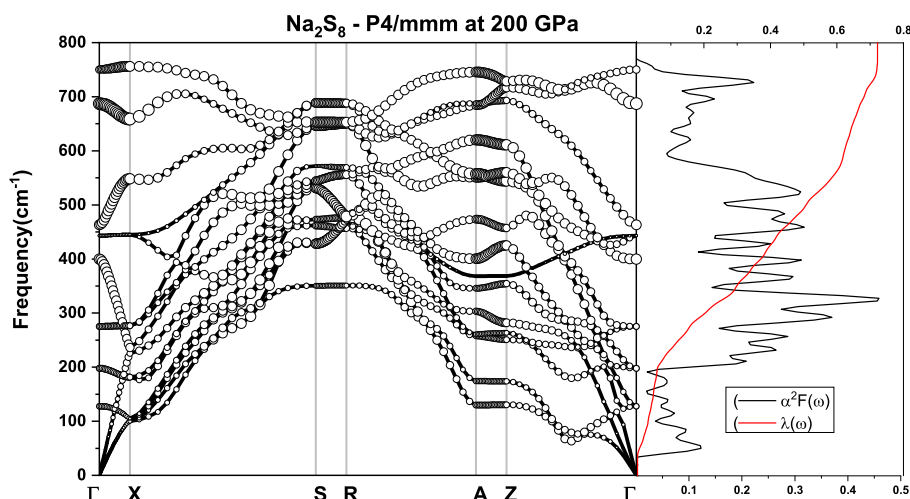


Figure 10. Phonon band structure, Eliashberg spectral function ($\alpha^2F(\omega)$), and the electron phonon integral ($\lambda(\omega)$) for $P4/mmm$ - Na_2S_8 at 200 GPa. Circles indicate the phonon linewidth with a radius proportional to the strength.

4. Conclusions

Evolutionary structure searches coupled with first-principles calculations have been employed to explore the phase diagram of sodium-rich and sodium-poor sulfides at 1 atm and within 100–200 GPa. At ambient pressure, the Na_2S_n , $n = 1, 2, 4, 5$, stoichiometries were thermodynamically stable, whereas $n = 3, 6, 8$ were low lying metastable species. In addition to identifying experimentally known or previously predicted species, we also found the novel $C2/c$ -II and $Imm2$ - Na_2S_3 phases, which differed in the orientation of the S_3^{2-} anions, as well as $C2$ - Na_2S_5 , which contained unbranched *trans* S_5^{2-} chains, and $C2$ - Na_2S_8 , which was comprised of S_8^{2-} helical-like chains. Even though the inclusion of van der Waals interactions did not have much of an impact on the optimized volumes of these phases, in some cases it did have an effect on the computed energy ordering of different polymorphs. Two dynamically stable sodium rich phases, $P\bar{3}m1$ - Na_3S and $Pmn2_1$ - Na_4S , whose enthalpies of formation lay ~ 70 meV/atom above the convex hull were also identified. Their structures were related to $Fm\bar{3}m$ - Na_2S , and they had intriguing electronic structures whose metallicity was derived from two-dimensional sodium sheets.

With the exception of the Na_2S stoichiometry, the high-pressure Na-S phase diagram has not been studied before. The stable and metastable sulfur-rich phases contained sulfur motifs that included atoms, dimers, V-shaped trimers, branched polymeric and zigzag chains, as well as two-dimensional corner-linked cyclohexane-like rings, and edge/corner-linked squares. At 200 GPa, the most stable Na_2S_n , $n = 3, 4, 6, 8$, phases were comprised of sodium nets and two-dimensional fused cube or square sulfur nets, whose electronic structure was interrogated. The Allen–Dynes modified McMillan formula was used to predict the superconducting critical temperature, T_c , of Na_2S_8 at 200 GPa, and it was found to be comparable to previous theoretical estimates for the β -Po sulfur phase, 15.5 K for the polysulfide vs. 16–19 K for elemental sulfur [91,92]. At 150–200 GPa, $P6_3/mmc$ - Na_3S and $Cmcm$ - Na_4S were found to be thermodynamically stable, and their structures differed from those proposed earlier for H_3S [37], Li_3S [35], K_3S [36], Li_4S [35], and K_4S [36] under pressure.

Supplementary Materials: The following are available online at <http://www.mdpi.com/2073-4352/9/9/441/s1>. Supplementary Materials include the structural coordinates, relative enthalpies, equation of states, volumes, zone-center vibrational frequencies at 0 GPa, electron localization functions, electronic band structures, densities of states, phonon band structures, and electron–phonon coupling parameters for the structures discussed in this paper. Other requests for materials should be addressed to E.Z. (ezurek@buffalo.edu).

Author Contributions: Conceptualization, E.Z.; validation, N.G., T.B., and Y.Y.; formal analysis, N.Z., N.G., T.B., Y.Y., and E.Z.; investigation, N.Z., N.G., T.B., and Y.Y.; resources, E.Z.; writing—original draft preparation, N.G.;

writing—review and editing, E.Z.; visualization, N.G., T.B., and Y.Y.; supervision, E.Z.; project administration, E.Z.; and funding acquisition, E.Z., and Y.Y.

Funding: E.Z. acknowledges the NSF (DMR-1827815) for funding. Support was provided by the Center for Computational Research at the University at Buffalo [93]. Y.Y. acknowledges the National Natural Science Foundation of China Grant No. 11404035, Jilin Provincial Natural Science Foundation of China Grant No. 20190201127JC, and Jilin Province Education Department “13th Five-Year” Science and Technology Research Project Grant No. JJKH20180941KJ.

Conflicts of Interest: The authors declare no conflict of interest.

References

1. Okamoto, H. The Li-S (lithium-sulfur) system. *J. Phase Equilib.* **1995**, *16*, 94–97. [[CrossRef](#)]
2. Janz, G.J.; Coutts, J.W.; Downey, J.R.; Roduner, E. Raman studies of sulfur-containing anions in inorganic polysulfides. Potassium polysulfides. *Inorg. Chem.* **1976**, *15*, 1755–1759. [[CrossRef](#)]
3. Sangster, J.; Pelton, A.D. The K-S (potassium-sulfur) system. *J. Phase Equilib.* **1997**, *18*, 82–88. [[CrossRef](#)]
4. Sangster, J.; Pelton, A.D. The Rb-S (rubidium-sulfur) system. *J. Phase Equilib.* **1997**, *18*, 97–100. [[CrossRef](#)]
5. Sangster, J.; Pelton, A.D. The Cs-S (cesium-sulfur) system. *J. Phase Equilib.* **1997**, *18*, 78–81. [[CrossRef](#)]
6. Oei, D.G. Sodium-sulfur system. I. Differential thermal analysis. *Inorg. Chem.* **1973**, *12*, 435–437. [[CrossRef](#)]
7. Sangster, J.; Pelton, A.D. The Na-S (sodium-sulfur) system. *J. Phase Equilib.* **1977**, *18*, 89–96. [[CrossRef](#)]
8. Rosen, E.; Tegman, R. A preparative and X-ray powder diffraction study of the polysulfides Na_2S_2 , Na_2S_4 and Na_2S_5 . *Acta Chem. Scand.* **1971**, *25*, 3329–3336. [[CrossRef](#)]
9. Föppel, H.; Busmann, E.; Frorath, F.K. Die kristallstrukturen von $\alpha\text{-Na}_2\text{S}_2$ und K_2S_2 , $\beta\text{-Na}_2\text{S}_2$ und Na_2Se_2 . *Z. Anorg. Allg. Chem.* **1962**, *314*, 12–20. [[CrossRef](#)]
10. Oei, D.G. Sodium-sulfur system. II. Polysulfides of sodium. *Inorg. Chem.* **1973**, *12*, 438–441. [[CrossRef](#)]
11. Böttcher, P.; Keller, R. Die kristallstruktur des $\alpha\text{-Na}_2\text{S}_5$ /The crystal structure of $\alpha\text{-Na}_2\text{S}_5$. *Z. Naturforsch. B* **1984**, *39*, 577–581. [[CrossRef](#)]
12. Weber, N. Ford gives Na-S battery details. *Chem. Eng. News* **1966**, *44*, 32–33.
13. Kummer, J.T.; Weber, N. Battery Having a Molten Alkali Metal Anode and Molten Sulfur Cathode. U.S. Patent 3,413,150, 26 November 1968.
14. Yao, Y.F.Y.; Kummer, J.T. Ion exchange properties of and rates of ionic diffusion in beta-alumina. *J. Inorg. Nucl. Chem.* **1967**, *29*, 2453–2475.
15. Ellis, B.L.; Nazar, L.F. Sodium and sodium-ion energy storage batteries. *Curr. Opin. Solid State Mater. Sci.* **2012**, *16*, 168–177. [[CrossRef](#)]
16. Hueso, K.B.; Armand, M.; Rojo, T. High temperature sodium batteries: Status, challenges and future trends. *Energy Environ. Sci.* **2013**, *6*, 734–749. [[CrossRef](#)]
17. Dunn, B.; Kamath, H.; Tarascon, J.M. Electrical energy storage for the grid: A battery of choices. *Science* **2011**, *334*, 928–935. [[CrossRef](#)] [[PubMed](#)]
18. Nikiforidis, G.; van de Sanden, M.C.M.; Tsampas, M.N. High and intermediate temperature sodium-sulfur batteries for energy storage: Development, challenges and perspectives. *RSC Adv.* **2019**, *9*, 5649–5673. [[CrossRef](#)]
19. Momida, H.; Yamashita, T.; Oguchi, T. First-principles study on structural and electronic properties of $\alpha\text{-S}$ and Na-S crystals. *J. Phys. Soc. Jpn.* **2014**, *83*, 124713. [[CrossRef](#)]
20. Mali, G.; Patel, M.U.M.; Mazaj, M.; Dominko, R. Stable crystalline forms of Na polysulfides: Experiment versus ab initio computational prediction. *Chem. Eur. J.* **2016**, *22*, 3355–3360. [[CrossRef](#)]
21. Wang, Y.; Hao, Y.; Xu, L.C.; Yang, Z.; Di, M.Y.; Liu, R.; Li, X. Insight into the discharge products and mechanism of room-temperature sodium-sulfur batteries: A first-principles study. *J. Phys. Chem. C* **2019**, *123*, 3988–3995. [[CrossRef](#)]
22. Zintl, E.; Harder, A.; Dauth, B. Gitterstruktur der oxyde, sulfide, selenide und telluride des lithiums, natriums und kaliums. *Z. Elektrochem. Angew. Phys. Chem.* **1934**, *40*, 588–593.
23. May, K. Die kristallstruktur des rubidium-sulfids Rb_2S . *Z. Kristallogr.* **1936**, *94*, 412–413. [[CrossRef](#)]
24. Sommer, H.; Hoppe, R. Die Kristallstruktur von Cs_2S . mit einer Bemerkung über Cs_2Se , Cs_2Te , Rb_2Se und Rb_2Te . *Z. Anorg. Allg. Chem.* **1977**, *429*, 118–130. [[CrossRef](#)]
25. Grzechnik, A.; Vegas, A.; Syassen, K.; Loa, I.; Hanfland, M.; Jansen, M. Reversible antifluorite to anticotunnite phase transition in Li_2S at high pressures. *J. Solid State Chem.* **2000**, *154*, 603–611. [[CrossRef](#)]

26. Vegas, A.; Grzechnik, A.; Syassen, K.; Loa, I.; Hanfland, M.; Jansen, M. Reversible phase transitions in Na₂S under pressure: A comparison with the cation array in Na₂SO₄. *Acta Crystallogr.* **2001**, *B57*, 151–156. [[CrossRef](#)]
27. Barkalov, O.I.; Naumov, P.G.; Felser, C.; Medvedev, S.A. Pressure-induced transition to Ni₂In-type phase in lithium sulfide(Li₂S). *Solid State Sci.* **2016**, *61*, 220–224. [[CrossRef](#)]
28. Santamaría-Pérez, D.; Vegas, A.; Muehle, C.; Jansen, M. High-pressure experimental study on Rb₂S: Antifluorite to Ni₂In-type phase transitions. *Acta Crystallogr.* **2011**, *B67*, 109–115. [[CrossRef](#)]
29. Santamaría-Pérez, D.; Vegas, A.; Muehle, C.; Jansen, M. Structural behaviour of alkaline sulfides under compression: High-pressure experimental study on Cs₂S. *J. Chem. Phys.* **2011**, *135*, 054511. [[CrossRef](#)]
30. Schön, J.C.; Čančarević, Ž.; Jansen, M. Structure prediction of high-pressure phases for alkali metal sulfides. *J. Chem. Phys.* **2004**, *121*, 2289–2304. [[CrossRef](#)]
31. Verma, A.K.; Modak, P.; Sharma, S.M. Structural phase transitions in Li₂S, Na₂S and K₂S under compression. *J. Alloy. Compd.* **2017**, *710*, 460–467. [[CrossRef](#)]
32. Li, Y.; Jin, X.; Cui, T.; Zhuang, Q.; Lv, Q.; Wu, G.; Meng, X.; Bao, K.; Liu, B.; Zhou, Q. Structural stability and electronic property in K₂S under pressure. *RSC Adv.* **2017**, *7*, 7424–7430. [[CrossRef](#)]
33. Yao, Y.; Tse, J.S. Superconducting hydrogen sulfide. *Chem. Eur. J.* **2018**, *24*, 1769–1778. [[CrossRef](#)]
34. Drozdov, A.P.; Eremets, M.I.; Troyan, I.A.; Ksenofontov, V.; Shylin, S.I. Conventional superconductivity at 203 kelvin at high pressures in the sulfur hydride system. *Nature* **2015**, *525*, 73–76. [[CrossRef](#)]
35. Kokail, C.; Heil, C.; Boeri, L. Search for high-*T_c* conventional superconductivity at megabar pressures in the lithium-sulfur system. *Phys. Rev. B* **2016**, *94*, 060502. [[CrossRef](#)]
36. Li, Y.; Jin, X.; Cui, T.; Zhuang, Q.; Zhang, D.; Meng, X.; Bao, K.; Liu, B.; Zhou, Q. Unexpected stable stoichiometries and superconductivity of potassium-rich sulfides. *RSC Adv.* **2017**, *7*, 44884–44889. [[CrossRef](#)]
37. Duan, D.; Liu, Y.; Tian, F.; Li, D.; Huang, X.; Zhao, Z.; Yu, H.; Liu, B.; Tian, W.; Cui, T. Pressure-induced metallization of dense (H₂S)₂H₂ with high-*T_c* superconductivity. *Sci. Rep.* **2014**, *4*, 6968. [[CrossRef](#)]
38. Lonie, D.C.; Zurek, E. XtalOpt: An open-source evolutionary algorithm for crystal structure prediction. *Comput. Phys. Commun.* **2011**, *182*, 372–387. [[CrossRef](#)]
39. XtalOpt. Available online: <http://xtalopt.github.io> (accessed on 19 August 2019).
40. Avery, P.; Falls, Z.; Zurek, E. XtalOpt Version r10: An open-source evolutionary algorithm for crystal structure prediction. *Comput. Phys. Commun.* **2017**, *217*, 210–211. [[CrossRef](#)]
41. Lonie, D.C.; Zurek, E. Identifying duplicate crystal structures: XtalComp, an open-source solution. *Comput. Phys. Commun.* **2012**, *183*, 690–697. [[CrossRef](#)]
42. Avery, P.; Zurek, E. RandSpG: An open-source program for generating atomistic crystal structures with specific spacegroups. *Comput. Phys. Commun.* **2017**, *213*, 208–216. [[CrossRef](#)]
43. Kresse, G.; Hafner, J. *Ab initio* molecular dynamics for liquid metals. *Phys. Rev. B* **1993**, *47*, 558–561. [[CrossRef](#)]
44. Kresse, G.; Joubert, D. From ultrasoft pseudopotentials to the projector augmented-wave method. *Phys. Rev. B* **1999**, *59*, 1758–1775. [[CrossRef](#)]
45. Maintz, S.; Deringer, V.L.; Tchougréeff, A.L.; Dronskowski, R. LOBSTER: A tool to extract chemical bonding from plane-wave based DFT. *J. Comput. Chem.* **2016**, *37*, 1030–1035. [[CrossRef](#)]
46. Perdew, J.P.; Burke, K.; Ernzerhof, M. Generalized gradient approximation made simple. *Phys. Rev. Lett.* **1996**, *77*, 3865–3868. [[CrossRef](#)]
47. Klimeš, J.; Bowler, D.R.; Michaelides, A. Chemical accuracy for the van der Waals density functional. *J. Phys. Condens. Matter* **2010**, *22*, 022201. [[CrossRef](#)]
48. Klimeš, J.; Bowler, D.R.; Michaelides, A. Van der Waals density functionals applied to solids. *Phys. Rev. B* **2011**, *83*, 195131. [[CrossRef](#)]
49. Blöchl, P.E. Projector augmented-wave method. *Phys. Rev. B* **1994**, *50*, 17953–17979. [[CrossRef](#)]
50. Parlinski, K.; Li, Z.Q.; Kawazoe, Y. First-principles determination of the soft mode in cubic ZrO₂. *Phys. Rev. Lett.* **1997**, *78*, 4063–4066. [[CrossRef](#)]
51. Chaput, L.; Togo, A.; Tanaka, I.; Hug, G. Phonon-phonon interactions in transition metals. *Phys. Rev. B* **2011**, *84*, 094302. [[CrossRef](#)]
52. Togo, A.; Tanaka, I. First principles phonon calculations in materials science. *Scr. Mater.* **2015**, *108*, 1–5. [[CrossRef](#)]

53. Giannozzi, P.; Baroni, S.; Bonini, N.; Calandra, M.; Car, R.; Cavazzoni, C.; Ceresoli, D.; Chiarotti, G.L.; Cococcioni, M.; Dabo, I.; et al. QUANTUM ESPRESSO: A modular and open-source software project for quantum simulations of materials. *J. Phys. Condens. Matter* **2009**, *21*, 395502. [[CrossRef](#)]
54. Dal Corso, A. Pseudopotentials periodic table: From H to Pu. *Comput. Mater. Sci.* **2014**, *95*, 337–350. [[CrossRef](#)]
55. Troullier, N.; Martins, J.L. Efficient pseudopotentials for plane-wave calculations. *Phys. Rev. B* **1991**, *43*, 1993–2006. [[CrossRef](#)]
56. Methfessel, M.; Paxton, A.T. High-precision sampling for Brillouin-zone integration in metals. *Phys. Rev. B* **1989**, *40*, 3616–3621. [[CrossRef](#)]
57. Allen, P.B.; Dynes, R.C. Transition temperature of strong-coupled superconductors reanalyzed. *Phys. Rev. B* **1975**, *12*, 905–922. [[CrossRef](#)]
58. Hanfland, M.; Loa, I.; Syassen, K. Sodium under pressure: Bcc to fcc structural transition and pressure-volume relation to 100 GPa. *Phys. Rev. B* **2002**, *65*, 184109. [[CrossRef](#)]
59. Gregoryanz, E.; Lundegaard, L.F.; McMahon, M.I.; Guillaume, C.; Nelmes, R.J.; Mezouar, M. Structural diversity of sodium. *Science* **2008**, *320*, 1054–1057. [[CrossRef](#)]
60. McMahon, M.I.; Gregoryanz, E.; Lundegaard, L.F.; Loa, I.; Guillaume, C.; Nelmes, R.J.; Kleppe, A.K.; Amboage, M.; Wilhelm, H.; Jephcoat, A.P. Structure of sodium above 100 GPa by single-crystal x-ray diffraction. *Proc. Natl. Acad. Sci. U. S. A.* **2007**, *104*, 17297–17299. [[CrossRef](#)]
61. Ma, Y.; Eremets, M.; Oganov, A.R.; Xie, Y.; Trojan, I.; Medvedev, S.; Lyakhov, A.O.; Valle, M.; Prakapenka, V. Transparent dense sodium. *Nature* **2009**, *458*, 182–185. [[CrossRef](#)]
62. Meyer, B. Elemental sulfur. *Chem. Rev.* **1976**, *76*, 367–388. [[CrossRef](#)]
63. Zakharov, O.; Cohen, M.L. Theory of structural, electronic, vibrational, and superconducting properties of high-pressure phases of sulfur. *Phys. Rev. B* **1995**, *52*, 12572–12578. [[CrossRef](#)]
64. Gavryushkin, P.N.; Litasov, K.D.; Dobrosmislov, S.S.; Popov, Z.I. High-pressure phases of sulfur: Topological analysis and crystal structure prediction. *Phys. Status Solidi B* **2017**, *254*, 1600857. [[CrossRef](#)]
65. Luo, H.; Greene, R.G.; Ruoff, A.L. β -Po phase of sulfur at 162 GPa: X-ray diffraction study to 212 GPa. *Phys. Rev. Lett.* **1993**, *71*, 2943–2946. [[CrossRef](#)]
66. Grimme, S. Semiempirical GGA-type density functional constructed with a long-range dispersion correction. *J. Comput. Chem.* **2006**, *27*, 1787–1799. [[CrossRef](#)]
67. Lozano, A.; Escribano, B.; Akhmatkaya, E.; Carrasco, J. Assessment of van der Waals inclusive density functional theory methods for layered electroactive materials. *Phys. Chem. Chem. Phys.* **2017**, *19*, 10133–10139. [[CrossRef](#)]
68. Perdew, J.P.; Ruzsinszky, A.; Csonka, G.I.; Vydrov, O.A.; Scuseria, G.E.; Constantin, L.A.; Zhou, X.; Burke, K. Restoring the density-gradient expansion for exchange in solids and surfaces. *Phys. Rev. Lett.* **2008**, *100*, 136406. [[CrossRef](#)]
69. Constantin, L.A.; Terentjevs, A.; Della Sala, F.; Fabiano, E. Gradient-dependent upper bound for the exchange-correlation energy and application to density functional theory. *Phys. Rev. B* **2015**, *91*, 041120. [[CrossRef](#)]
70. Peng, H.; Perdew, J.P. Rehabilitation of the Perdew-Burke-Ernzerhof generalized gradient approximation for layered materials. *Phys. Rev. B* **2017**, *95*, 081105. [[CrossRef](#)]
71. Terentjev, A.V.; Constantin, L.A.; Pitarke, J. Dispersion-corrected PBEsol exchange-correlation functional. *Phys. Rev. B* **2018**, *98*, 214108. [[CrossRef](#)]
72. Peng, H.; Yang, Z.H.; Perdew, J.P.; Sun, J. Versatile van der Waals density functional based on a meta-generalized gradient approximation. *Phys. Rev. X* **2016**, *6*, 041005. [[CrossRef](#)]
73. Rettig, S.J.; Trotter, J. Refinement of the structure of orthorhombic sulfur, α -S₈. *Acta Cryst.* **1987**, *C43*, 2260–2262. [[CrossRef](#)]
74. Wagman, D.D.; Evans, W.H.; Parker, V.B.; Schumm, R.H.; Halow, I.; Bailey, S.M.; Churney, K.L.; Nuttall, R.L. The NBS tables of chemical thermodynamic properties. *J. Phys. Chem. Ref. Data* **1982**, *11* (Suppl. 2), 1–392.
75. Tegman, R. The crystal structure of sodium tetrasulphide, Na₂S₄. *Acta Cryst.* **1973**, *B29*, 1463–1469. [[CrossRef](#)]
76. Kelly, B.; Woodward, P. Crystal structure of dipotassium pentasulphide. *J. Chem. Soc. Dalton Trans.* **1976**, 1314–1316. [[CrossRef](#)]

77. Böttcher, P. Synthesis and crystal structure of the dirubidiumpentachalcogenides Rb_2S_5 and Rb_2Se_5 . *Z. Kristallogr. Cryst. Mater.* **1979**, *150*, 65–73. [[CrossRef](#)]
78. Böttcher, P.; Kruse, K. Darstellung und kristallstruktur von dicaesiumpentasulfid (Cs_2S_5). *J. Less Common Met.* **1982**, *83*, 115–125. [[CrossRef](#)]
79. Janz, G.J.; Downey, J.R.; Roduner, E.; Wasilczyk, G.J.; Coutts, J.W.; Eluard, A. Raman studies of sulfur-containing anions in inorganic polysulfides. Sodium polysulfides. *Inorg. Chem.* **1976**, *15*, 1759–1763. [[CrossRef](#)]
80. Te Velde, G.; Bickelhaupt, F.M.; Baerends, E.J.; Fonseca Guerra, C.; van Gisbergen, S.J.A.; Snijders, J.G.; Ziegler, T. Chemistry with ADF. *J. Comput. Chem.* **2001**, *22*, 931–967. [[CrossRef](#)]
81. ADF2018. SCM, Theoretical Chemistry, Vrije Universiteit, Amsterdam, The Netherlands. Available online: <http://www.scm.com> (accessed on 19 August 2019).
82. Feng, J.; Hennig, R.G.; Ashcroft, N.; Hoffmann, R. Emergent reduction of electronic state dimensionality in dense ordered Li-Be alloys. *Nature* **2008**, *451*, 445–458. [[CrossRef](#)]
83. Miao, M. Helium chemistry: React with nobility. *Nat. Chem.* **2017**, *9*, 409–410. [[CrossRef](#)]
84. Liu, Z.; Botana, J.; Hermann, A.; Zurek, E.; Yan, D.; Lin, H.; Miao, M. Reactivity of He with ionic compounds under high pressure. *Nat. Commun.* **2018**, *9*, 951. [[CrossRef](#)]
85. Zarifi, N.; Liu, H.; Tse, J.S.; Zurek, E. Crystal structures and electronic properties of Xe-Cl compounds at high pressure. *J. Phys. Chem. C* **2018**, *122*, 2941–2950. [[CrossRef](#)]
86. Mishra, A.K.; Muramatsu, T.; Liu, H.; Geballe, Z.M.; Somayazulu, M.; Ahart, M.; Baldini, M.; Meng, Y.; Zurek, E.; Hemley, R.J. New calcium hydrides with mixed atomic and molecular hydrogen. *J. Phys. Chem. C* **2018**, *122*, 19370–19378. [[CrossRef](#)]
87. Gregoryanz, E.; Degtyareva, O.; Somayazulu, M.; Hemley, R.J.; Mao, H.K. Melting of dense sodium. *Phys. Rev. Lett.* **2005**, *94*, 185502. [[CrossRef](#)]
88. Neaton, J.B.; Ashcroft, N.W. On the constitution of sodium at higher densities. *Phys. Rev. Lett.* **2001**, *86*, 2830–2833. [[CrossRef](#)]
89. Tutchton, R.; Chen, X.; Wu, Z. Is sodium a superconductor under high pressure? *J. Chem. Phys.* **2017**, *146*, 014705. [[CrossRef](#)]
90. Struzhkin, V.V.; Hemley, R.J.; Mao, H.K.; Timofeev, Y.A. Superconductivity at 10–17 K in compressed sulphur. *Nature* **1997**, *390*, 382–384. [[CrossRef](#)]
91. Rudin, S.P.; Liu, A.Y. Predicted simple-cubic phase and superconducting properties for compressed sulfur. *Phys. Rev. Lett.* **1999**, *83*, 3049–3052. [[CrossRef](#)]
92. Monni, M.; Bernardini, F.; Sanna, A.; Profeta, G.; Massidda, S. Origin of the critical temperature discontinuity in superconducting sulfur under high pressure. *Phys. Rev. B* **2017**, *95*, 064516. [[CrossRef](#)]
93. Center for Computational Research, University at Buffalo. Available online: <http://hdl.handle.net/10477/79221> (accessed on 19 August 2019).



© 2019 by the authors. Licensee MDPI, Basel, Switzerland. This article is an open access article distributed under the terms and conditions of the Creative Commons Attribution (CC BY) license (<http://creativecommons.org/licenses/by/4.0/>).